JOURNAL OF GEOPHYSICAL RESEARCH, VOL. 106, NO. A7, PAGES 12,903–12,917, JULY 1, 2001

A semiempirical equatorial mapping of AMIE convection electric potentials (MACEP) for the January 10, 1997, magnetic storm

A. Boonsiriseth,[1] R. M. Thorne,[1] G. Lu,[2] V. K. Jordanova,[3] M. F. Thomsen,[4] D. M. Ober,[5] and A. J. Ridley,[6]

Abstract. Owing to satellite and instrumental limitations, in situ magnetospheric electric field measurements are only available at isolated locations during storm time conditions. A global view of the inner magnetospheric convection electric field can be obtained by mapping ionospheric potentials into the equatorial plane. A mapping procedure for assimilative mapping of ionospheric electrodynamics (AMIE) ionospheric potentials (MACEP) is used to obtain convection patterns for the January 10, 1997, magnetic storm. The results are compared with the widely used empirical Volland-Stern model and the mapping of Weimer ionospheric potentials. While the gross temporal evolution of the large-scale potential drop across the magnetosphere is similar in all three models, detailed intercomparison shows that the MACEP procedure is capable of resolving highly variable and relatively small scale features of the electric field that are not treated by the Volland-Stern model nor seen from the Weimer mapping. The MACEP results are in reasonable agreement with limited electric field measurements from the electric field instrument on the Polar spacecraft and LANL measurements of thermal ion velocities at geosynchronous orbit during prestorm and recovery phase conditions. However, the inner boundary condition employed in the current version of AMIE is unable to reproduce the magnitude of the penetrating electric fields observed in the inner magnetosphere during the main phase of a storm. The addition of a penetration electric field associated with an asymmetric ring current in the dusk sector improved MACEP results at the duskside low-L region.

1. Introduction

An enhanced convection electric field plays a dominant role in the injection and energization of ring current particles during the main phase of a magnetic storm [*Lyons and Williams*, 1980] and dayside particle loss to the magnetopause during the recovery phase [*Kozyra et al.*, 1997; *Jordanova et al.*, 1998]. A realistic time-dependent global model for the inner magnetospheric convection electric field is required to successfully model the evolution of the ring current and the dynamics of the inner magnetosphere during a storm. Previous modeling efforts on storm time ring current dynamics have been limited by the use of empirical models (e.g., the Volland-Stern model [*Volland*, 1973; *Stern*, 1975; *Maynard and Chen*, 1975]) for the convection electric field. Here we attempt to improve the specification of convection electric field variation during the January 10, 1997, storm by using ionospheric potentials generated by assimilative mapping of ionospheric electrodynamics (AMIE) [*Richmond*, 1992]. The *Tsyganenko* [1996] magnetic field model is used to map the potentials to the equatorial region over the range L = 2.5 to 6.5.

In situ electric field data obtained by using the double-probe technique (integrated over the width of the magnetosphere to obtain large-scale electric field) and the electron gun instrument have been studied previously by *Maynard et al.* [1983], *Baumjohann et al.* [1985], *Wygant et al.* [1998], and *Rowland and Wygant* [1998] for specific data sets under different solar wind conditions. *Maynard et al.* [1982, 1983] studied a 1-year data set from ISEE 1; they found extremely variable electric field during moderately high magnetic activity for the region L = 2-6. Their results also indicated a

[1]Department of Atmospheric Sciences, University of California, Los Angeles, Los Angeles, California.
[2]High Altitude Observatory, Boulder, Colorado.
[3]University of New Hampshire, Durham, New Hampshire
[4]Los Alamos National Laboratory, Los Alamos, New Mexico.
[5]Mission Research Corporation, Nashua, New Hampshire.
[6]Space Research, University of Michigan, Ann Arbor, Michigan.

Paper number 1999JA000332.
0148-0227/01/1999JA000332$09.00

penetration of the convection field into $L \leq 4$ during disturbed times in the late evening and early morning regions. However, their data were sparse and limited to the plasmaspheric region. Since the double-probes instrument could not operate in eclipse, their coverage of the near-midnight region was poor. ISEE 1 also took 1 year to cover all local times, introducing seasonal effects into their data set. *Baumjohann et al.* [1985] used data obtained from the Electron Gun Experiment on GEOS 2 to study the average convective electric field patterns at $L = 6.6$ during moderate (Kp = 0-4) conditions. They discovered ionospheric conductivity influences on the equatorial magnetosphere related to local time asymmetry in the flow patterns of plasma during moderately disturbed times. The results were confined to geosynchronous orbit, and the usable data were futher limited to the dayside (0900-1800 LT) region during disturbed times, owing to the stretching of magnetic field lines on the nightside which affected the injection angle of the electron gun. Most recently, *Wygant et al.* [1998] and *Rowland and Wygant* [1998] studied in situ electric field data obtained from CRRES for a 10-month period in 1991. Their data, which had a substantial radial coverage from $L = 2.5$ to $L = 8.5$ and a broad local time coverage (1200 to 0400 LT, eastward), coincided with solar maximum conditions and included six major storms with Dst of less than -100 nT and a wide range of Kp values (0 to 9-). Because of the orientation of the double probes on CRRES, the instrument was unable to provide measurements for the electric field in the Sun-Earth direction. *Wygant et al.* [1998] based their study on the March 24, 1991, storm.

In situ observations, despite their importance, are unable to provide a global description of the inner magnetospheric electric field. Consequently, simplified empirical models (e.g., the Volland-Stern model) for large-scale electric field potentials have been constructed for use in storm time ring current modeling. Variations on the Volland-Stern electric field model have been used by *Chen et al.* [1994], *Jordanova et al.* [1997], and *Kozyra et al.* [1997] to follow the temporal evolution of the storm time ring current. These electric field models give a realistic description of the overall potential drop across the magnetosphere under different levels of magnetic activity, but they are highly idealized and do not take into account the intricate spatial structures and rapid temporal evolution of the magnetospheric electric field during geomagnetic storms. *Baumjohann et al.* [1985] found that during very quiet conditions (Kp = 0-1) the electric potentials seen by GEOS 2 do not follow the Volland-Stern potentials. Furthermore, the standard Volland-Stern model predicts strong shielding in the inner region of the magnetosphere where *Rowland and Wygant* [1998] saw the strongest fields.

To model the development of the storm time ring current, *Chen et al.* [1994] included both a Volland-Stern type steady state electric field and a time-dependent component. Their time-dependent electric field is generated from a series of quasi-random cross-tail potential enhancements of 3-, 6-, and 12-hour prototypical storms. In earlier studies, *Fok et al.* [1995] and *Jordanova et al.* [1997] had also used a Kp-dependent Volland-Stern electric field model to drive their ring current models. In order to simulate the ring current evolution during the January 10-11, 1997, storm with their ring current-atmosphere interaction model (RAM) code, *Jordanova et al.* [1999a] used an interplanetary magnetic field (IMF) dependent Volland-Stern model. This model was based on the polar cap potential drop calculated with the Weimer ionospheric potential model. Weimer ionospheric potentials are derived from statistical smoothing of data from many random satellite passes [*Weimer*, 1995, 1996]. The electric field used most recently by *Kistler et al.* [1999] and *Jordanova et al.* [1999b] is generated by using a method of mapping ionospheric potentials onto the equatorial plane during times of interest. The ionospheric potentials used in their mapping are derived from *Weimer*'s [1996] convection model. The magnetic field model used for mapping was either a dipole field [*Kistler et al.*, 1999] or the Tsyganenko 1996 magnetic field model [*Jordanova et al.*, 1999b]. A mapping procedure similar to that of *Jordanova et al.* [1999b], but based on AMIE ionospheric electric potentials, is used in the present study to obtain the inner magnetospheric electric potentials for the January 10, 1997, geomagnetic storm.

2. MACEP, Global Distribution of Magnetospheric Electric Field

Mapping of AMIE convection electric potentials (MACEP) is a procedure which maps ionospheric potentials produced by AMIE along magnetic field lines to generate the inner magnetospheric equatorial convection potentials. The magnetic field model used in MACEP is the Tsyganenko 1996 magnetic field model. Results produced by MACEP throughout the geomagnetic storm on January 10, 1997, will be compared with the standard Kp-dependent Volland-Stern model and Weimer electric potential patterns. Thermal ion velocities taken from two geosynchronous Los Alamos National Laboratory (LANL) satellites will be employed to test the reliability of the MACEP derived convection flow patterns at geosynchronous orbit. In situ electric field measurements from the electric field instrument (EFI) on Polar will also be compared with electric fields calculated from the MACEP potentials for two periods during the January 10, 1997, storm. All potential patterns and electric fields presented in this paper, together with the LANL velocity data, are in the corotation frame of reference.

2.1. AMIE Procedure

The AMIE procedure involves the synthesis of data from a variety of sources. The data are applied to a weighted least squares fit to produce an overall iono-

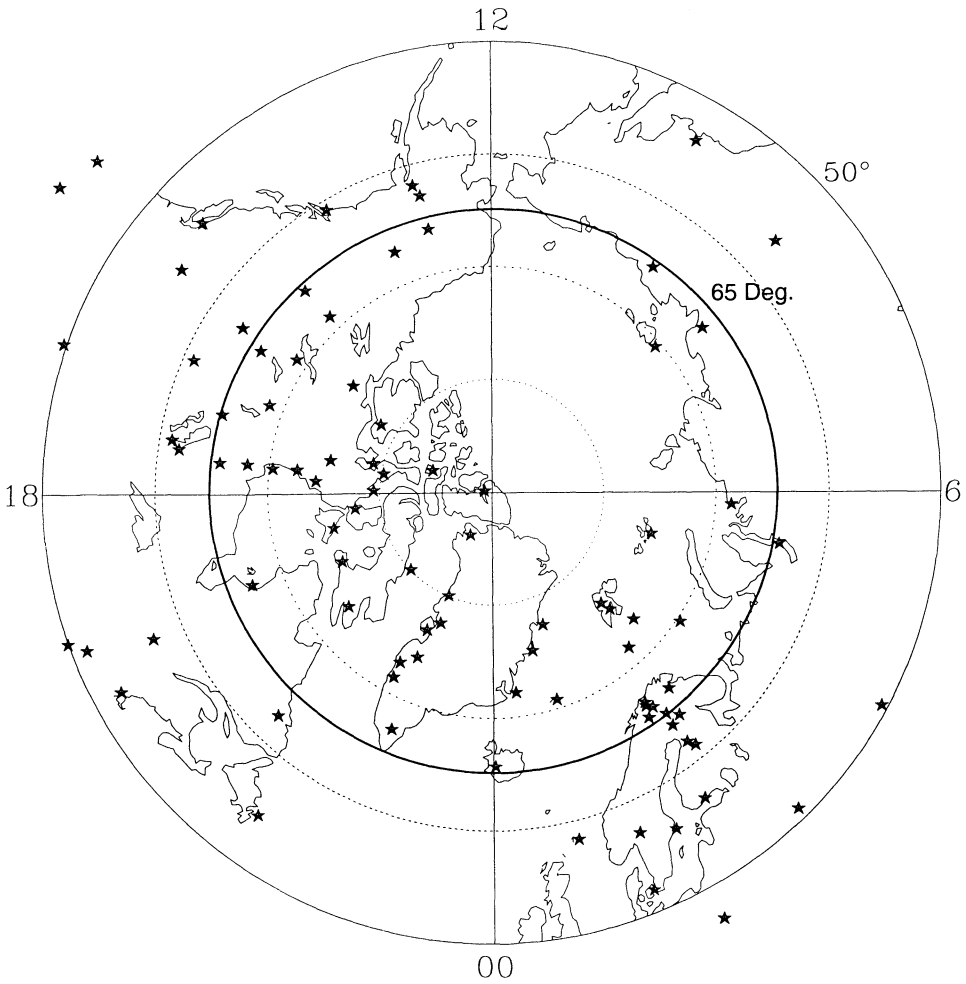

Figure 1. Ground magnetometer coverage on January 10, 1997, at 0100 UT. The region of the MACEP study extends from 50° to 66.5° magnetic latitude. The local time regions with poor magnetometer coverage are at (UT + 4) MLT to (UT + 71) MLT and (UT + 22) MLT to (UT + 23) MLT.

spheric electric potential pattern. This procedure ensures that the less reliable observations contribute less to the results [*Richmond*, 1992]. Data used as input in AMIE during the January 10, 1997, storm include auroral conductances derived from the Polar UVI image, six SuperDARN radars, two NOAA satellites, three DMSP satellites, and 119 ground magnetometers, although not all of the data were neccessarily available at a given location during a given time. On January 10, 1997, the Polar UVI images were available from 1000 UT to 2300 UT, all six SuperDARN radars were operating the entire day, and the polar-orbiting Sun-synchronous NOAA and DMSP satellites were orbiting on a period of 110 min. Figure 1 shows the distributions of the ground magnetometers that were operating during the January 10 storm at 0100 UT. There is very good coverage for high latitudes but limited coverage at midlatitudes (50°-66.5°). Between 50° and 66.5°, there is no magnetometer coverage for a 2-hour period (2200-2400 MLT) over the Atlantic and a 3-hour period (0500-800 MLT) over Siberia. Thus as the Earth rotates, the MLT regions with poor magnetometer coverage lie within (UT + 4) MLT to (UT + 7) MLT and (UT + 21) MLT to (UT + 23) MLT. For such regions, the AMIE potential patterns are mainly generated on the basis of a statistical model [*Foster et al.*, 1986] as well as extrapolation of the fitting from adjacent data. Owing to the lack of observations, it is not possible to assess the reliability of the AMIE potentials over those regions. The region of AMIE potential patterns in the ionosphere extends from 50° to 90° invariant latitude in steps of 1.67° in the Northern Hemisphere and includes all MLT in steps of every 10°. The MACEP procedure discussed here utilizes AMIE potentials from 50° to 66.5° invariant latitude range which map to the dominant region of the storm time ring current between $L = 2.5$ and $L = 7$.

In the high-latitude region, a number of assumptions can be made which simplify the AMIE technique, such as the magnetic field lines being vertical. At lower latitudes, this assumption breaks down and a more rigorous approach is needed. In addition, the boundary condi-

tions employed in the AMIE technique require that the electric potential at the lowest latitude must be sloped toward zero. These two conditions make modeling disturbed time periods less accurate. During a magnetic storm, the auroral oval can extend down to 55° magnetic latitude or lower. In this region, the dipole tilt is approximately 35°, which invalidates the vertical field line approximation. In addition, the lower boundary of AMIE is within 10° of this location; so strong penetration fields can be supressed by the boundary condition.

An attempt at improving the limitations of AMIE has been made in this study by an addition of an empirical model of penetration electric fields developed by *Ridley et al.* [2000] on the basis of field-aligned currents obtained from the RAM code [*Liemohn et al.*, 2001; M. W. Liemohn et al., The asymmetry of the storm time current in the inner magnetosphere, submitted to *Journal of Geophysical Research*, 2000]. The model was produced by taking the region 2 currents derived from the RAM code and mapping them to the ionosphere by using a simple dipole field. The currents were combined with conductance patterns consistent with the input field-aligned currents, and a series of potential patterns were derived. These patterns remain similar in shape during the magnetic storm, but the magnitude of the potential varies as *Dst* changes. The patterns were averaged and normalized to create a penetration electric field pattern, and a relationship was determined for the magnitude of the potential to the *Dst* index. This relationship includes both an injection phase (*Dst* is decreasing) and a recovery phase (*Dst* is increasing). The relationship results in an approximately 90% correlation between the modeled cross polar cap potential and the empirically derived value based on *Dst*. In the study of A. J. Ridley and M. W. Liemohn (A model-derived penetration electric field description, submitted to *Journal of Geophysical Research*, 2000) the data-model comparison indicated that the patterns should be rotated from the true location of the penetration field. In the current study we compensate for this by rotating their patterns in MLT by 90° westward to better fit the data.

All MACEP patterns shown in this study include the addition of the empirical penetration electric field with a 90° westward rotation. The results of the MACEP patterns compared best with data when the empirical penetration electric field is strongest in the dusk sector. This indicates that the divergence of the asymmetric ring current should peak in the dusk sector. MACEP patterns (with and without the addition of the penetration electric field) will be compared with in situ data measurements from LANL satellites and the Polar satellite.

2.2. Tsyganenko 1996 Magnetic Field Model

The magnetic field model used by both MACEP and the Weimer mapping is the Tsyganenko 1996 model [*Tsyganenko*, 1996]. The solar wind velocity V_{sw}, density n_{sw}, and components of the interplanetary field (B_y and B_z) during the January 10 storm were obtained by the Solar Wind Experiment (SWE) [*Ogilvie et al.*, 1995] and MFI [*Lepping et al.*, 1995] instruments on the Wind spacecraft. The solar wind dynamic pressure, B_x, B_y, and B_z for January 10 are plotted in Figure 2, together with the pressure-corrected *Dst** index. On that day, Wind was approximately 104 R_E upstream of the magnetopause, and the average solar wind velocity was ~450 km/s [*Farrugia et al.*, 1998], giving a delay time of approximately 0.4 hour for solar wind features seen at Wind to reach the magnetopause. The interplanetary magnetic field data used to generate Weimer 1996 ionospheric electric potentials were delayed by 30 min and averaged over 40-min periods prior to the specified universal time, in order to account for ionospheric plasma convection response time to solar wind changes. To be consistent with this, a time delay of 30 min was imposed on the solar wind data used in the Tsyganenko 1996 model for both MACEP and Weimer mappings in the present study.

The Tsyganenko 1996 magnetic field tends to produce an overestimation of the field values near the high-latitude cusps and near-tail equatorial regions [*Zhou et al.*, 1997], but low-latitude regions (<66.5°) of the Earth's magnetosphere appropriate for this study are generally well represented by this magnetic field model. For very large geomagnetic storms (*Dst* $\ll$ -100 nT) the inner region magnetic field may be distorted owing to the large dynamic pressure of the solar wind. Under extremely intense storm conditions, the Tsyganenko 1996 magnetic field model may not be able to accurately represent the magnetic field. However, for the January 10, 1997, storm *Dst* remained above -100 nT throughout the storm period. In this case, the Tsyganenko 1996 model is sufficiently accurate for modeling the magnetic field in the region of interest (inner magnetosphere) to this study.

3. MACEP Results

AMIE electric potential patterns in the corotation frame are available with 5-min resolution generated from data taken within ±3 min of the given UT times. The corresponding equatorial electric potential patterns obtained by using the MACEP procedure for January 10, 1997, are shown at half-hour intervals during different phases of the storm in Figure 3 (sudden commencement phase), Figure 4 (main phase), and Figure 5 (recovery phase). The plots shown are instantaneous and have not been averaged; so we can study rapidly varying features seen in the electric potentials. Thus some time-varying features may seem to be unrelated to the previous plot. Note that Figures 3, 4, and 5 are plotted by using different gray scales.

Some notable features seen in Figure 3 during the sudden commencement phase of the storm are the initial penetration of convection on the nightside to low L

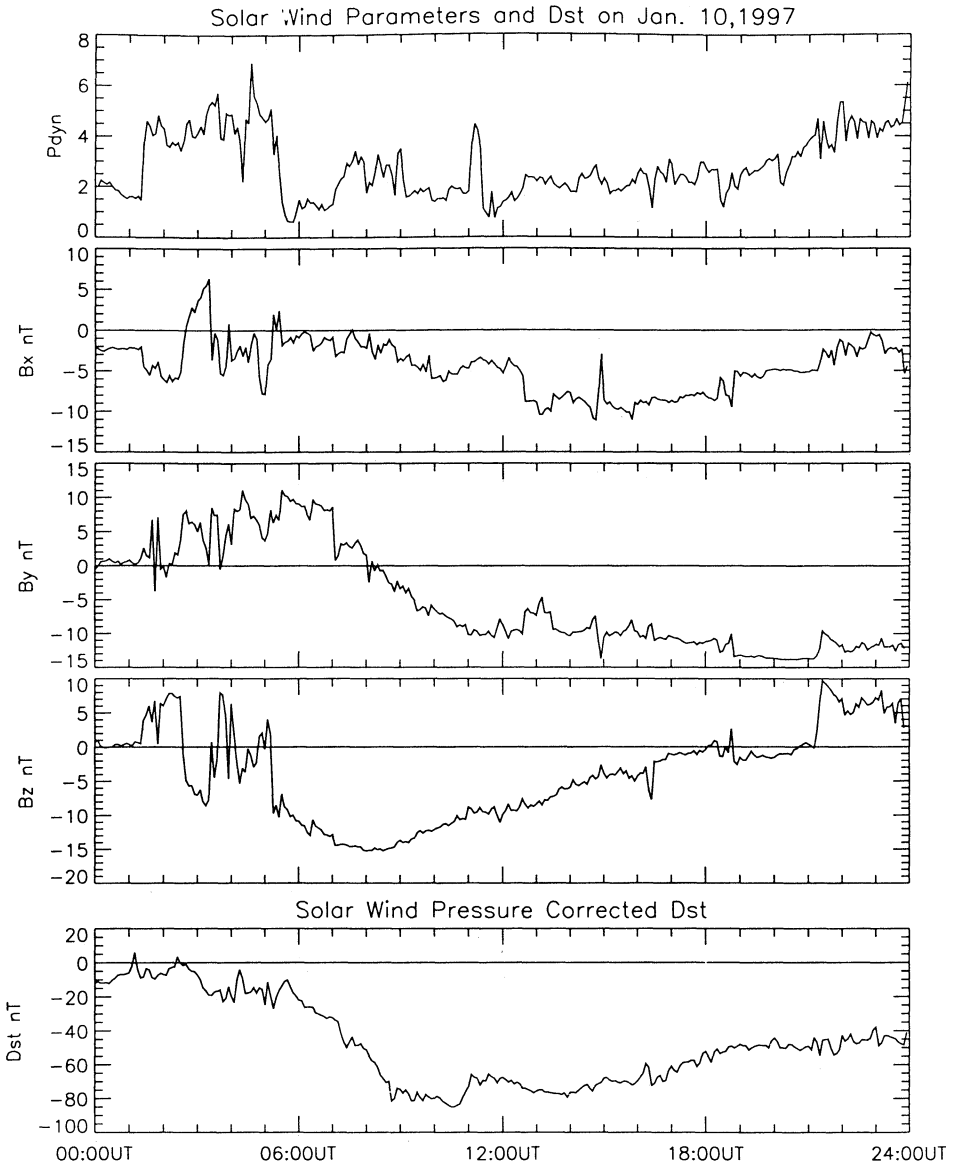

Figure 2. Five-minute resolution solar wind data and solar wind pressure corrected *Dst* for January 10, 1997.

values at 0230 UT which corresponds to the first large drop in B_z from positive to negative values. The nightside convection electric field intensifies at 0300 UT, as B_z continues to decrease to larger negative values. At 0500 UT a strong but transient dusk-to-dawn electric field develops at low L on a very rapid timescale. The dusk-to-dawn electric field disappears after less than 30 min and is probably related to the "overshielding electric field" described by *Wolf* [1983]. Figure 3 also shows a westward rotation of the symmetry axis of the potential pattern from the dawn-to-dusk direction to earlier local times during the moderately enhanced dawn-to-dusk electric field event at 0230-0300 UT. However, at 0400 UT the symmetry axis rotated to later local times (eastward). There is also a day/night asymmetry associated with both the dawn-to-dusk and dusk-to-dawn electric field, as is seen at 0230 UT, 0300 UT, 0400 UT, and 0500 UT. Convection at low L values appears to be stronger on the nightside magnetosphere.

Throughout the main phase (Figure 4) of the storm (0600-1130 UT), which is characterized by strong negative B_z (Figure 2), the electric field patterns are highly variable in both direction and magnitude. This is consistent with the turbulent electric fields measured by ISEE 1 during magnetically disturbed periods when $Kp \geq 5$ [*Maynard et al.*, 1982] and the strongly fluctuating electric fields (in both magnitude and direction) on timescales of 15 min to an hour observed during the March 24, 1991, storm by *Wygant et al.* [1998]. Convection intensifies at 0600 UT and the electric field is notably stronger on the nightside, characterized by a larger gradient in the electric potentials. Large convec-

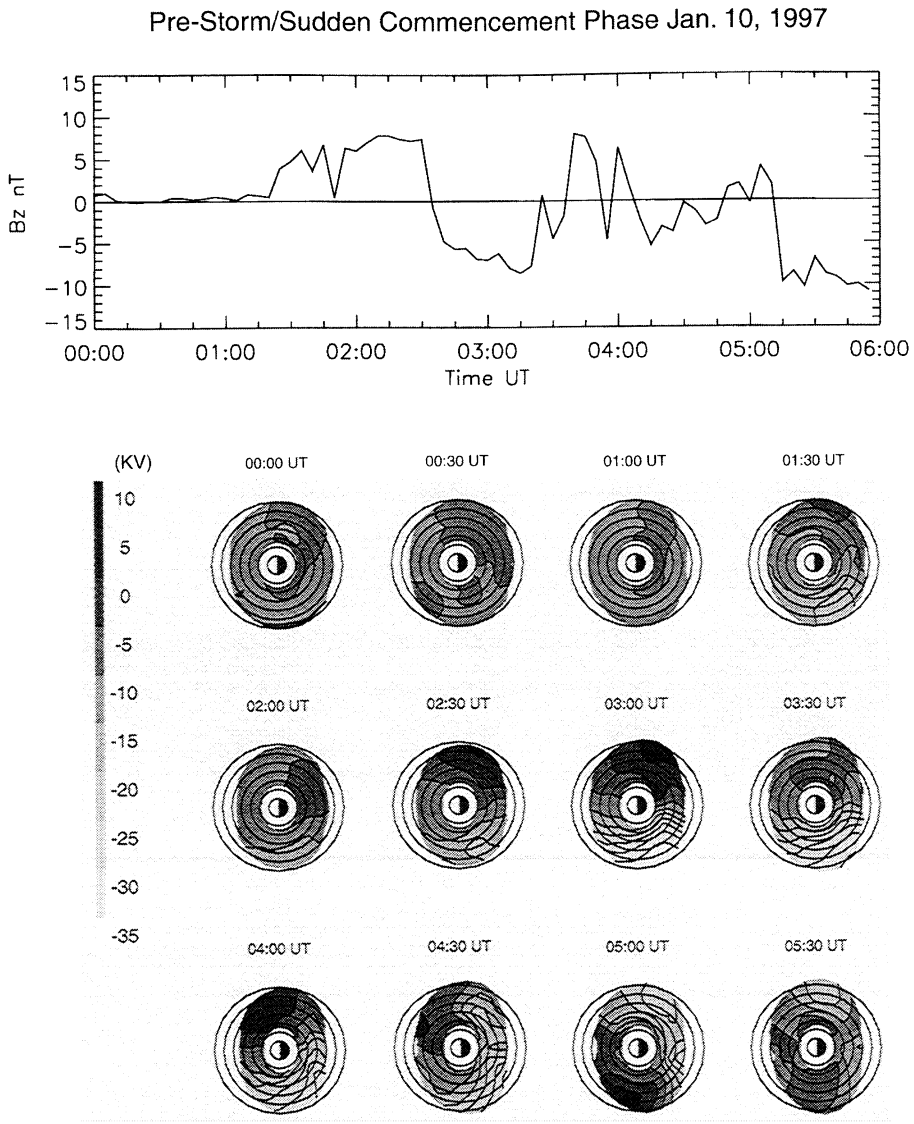

Figure 3. MACEP equatorial electric potential patterns plotted in the corotation frame at 30-min intervals during the sudden commencement phase of the January 10, 1997, magnetic storm. For each dial plot the Sun is to the left and the circles depict L shells from 1 to 7. The scale of the potential variation is given on the left, and the interplanetary B_z variation for the interval covered is plotted above.

tive flow on the nightside has been observed by *Wygant et al.* [1998] at $L = 4$ during both the main and recovery phases of the March 24, 1991, storm. As B_z continues to decrease to larger negative values, the *Dst* depression intensifies and there is further penetration of both dayside and nightside convection until about 0930 UT, when B_z stops decreasing and starts to increase to less negative values. During highly disturbed conditions, starting at 0700 UT, the symmetry axis rotates (~5 hours) eastward to much later local times. Contrary to the predictions of electric field shielding at low L (e.g., as specified in the Volland-Stern model), the MACEP electric fields tend to maximize at lower L ($\approx$3) during the most disturbed phase of the storm. This is consistent with the earlier CRRES results of *Rowland and Wygant* [1998]. During the main phase of the March 24, 1991 storm, *Wygant et al.* [1998] observed the strongest enhanced convection (large E_y) in the nightside dusk quadrant (1800-2100 LT) at L values between $L = 2$ and $L = 4$. However, between 0700 UT and 0930 UT the MACEP patterns indicate that the largest dawn-dusk electric field (largest electric potential gradient in the dawn-dusk direction in MACEP patterns) appears to be on the dayside dusk quadrant. This apparent discrepency with the *Wygant et al.* [1998] results may be partially due to the fact that the CRRES satellite did not sample the dayside dusk quadrant during the main phase of the March 24, 1991, storm.

The recovery phase (Figure 5) of the storm begins soon after 1100 UT, but *Dst* does not reach prestorm

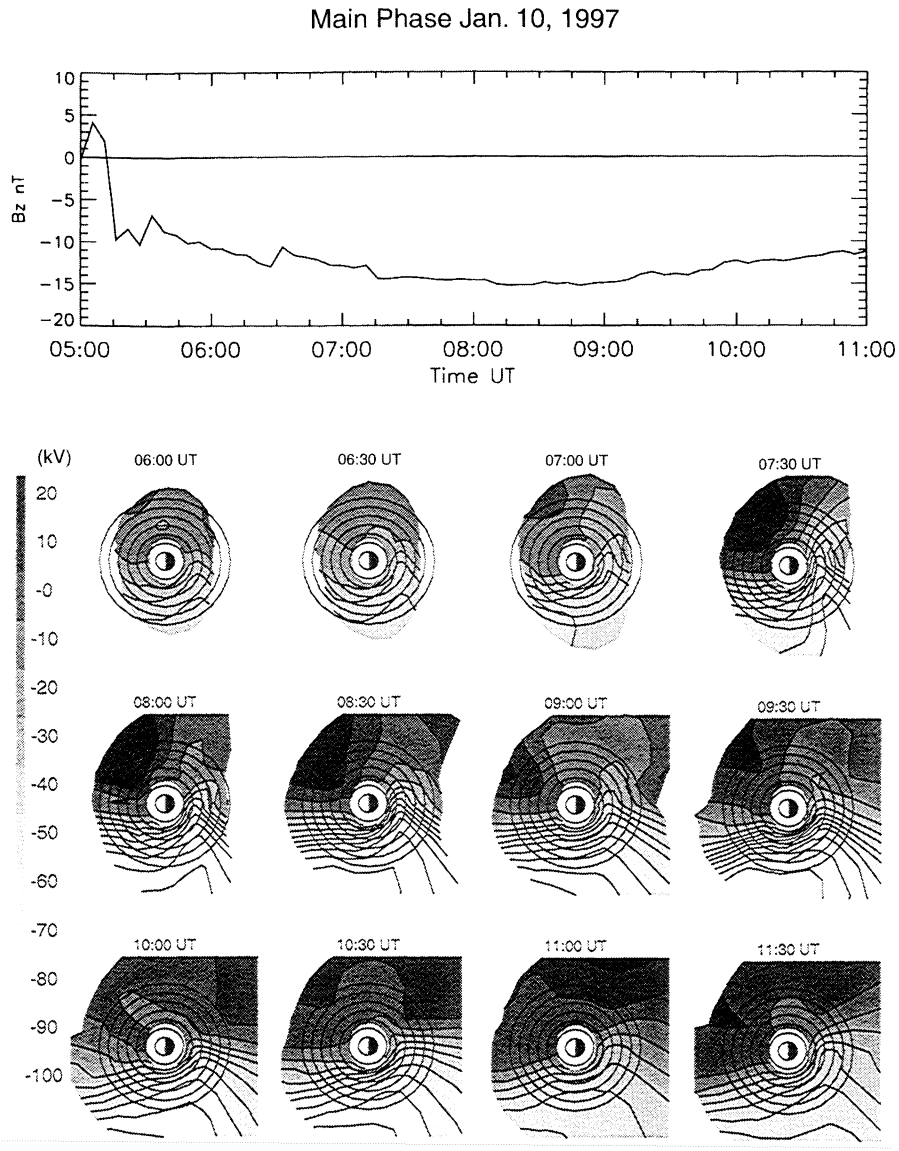

Figure 4. Dial plots of the MACEP equatorial potentials in the corotation frame for the storm main phase.

values for several days. The axis of symmetry once again rotates to earlier local times (1530-1700 UT and 1900-2030 UT), as the magnetosphere returns to more moderate conditions. Another interesting feature is a region of potential enhancement that develops in the premidnight/evening sector during the recovery phase of the storm, seen in frames 1830 UT, 1930 UT, and 2100 UT in Figure 5. This feature may be related to polarization jets observed in the ionosphere [*Foster and Rich*, 1998]. Polarization jets have been associated with northward and eastward electric field signatures in the ionosphere in the premidnight sector during geomagnetic storms causing an uplift of the F layer ionosphere. A northward electric field will map to the magnetosphere as a radially directed electric field, consistent with the radial electric field seen in MACEP in the premidnight sector. The eastward electric field is also seen in MACEP at a slightly later local time associated with the same enhanced potential region. A study is currently under way to further examine the relationship between the magnetospheric enhanced potential region and ionospheric features such as polarization jets.

4. Comparison of MACEP Convection With LANL Data

Thermal ion (<100 eV) velocities obtained from two LANL geosynchronous satellites 1991-080 (~70°E) and 1994-084 (~103°E) during January 10, 1997, are plotted in the corotation frame in Figure 6a and Figure 6b. Exhibited data are mainly restricted to the dayside portion of their orbit, where the measured density was well above background and the signal-to-noise ratio is relatively high. High-velocity data have a higher con-

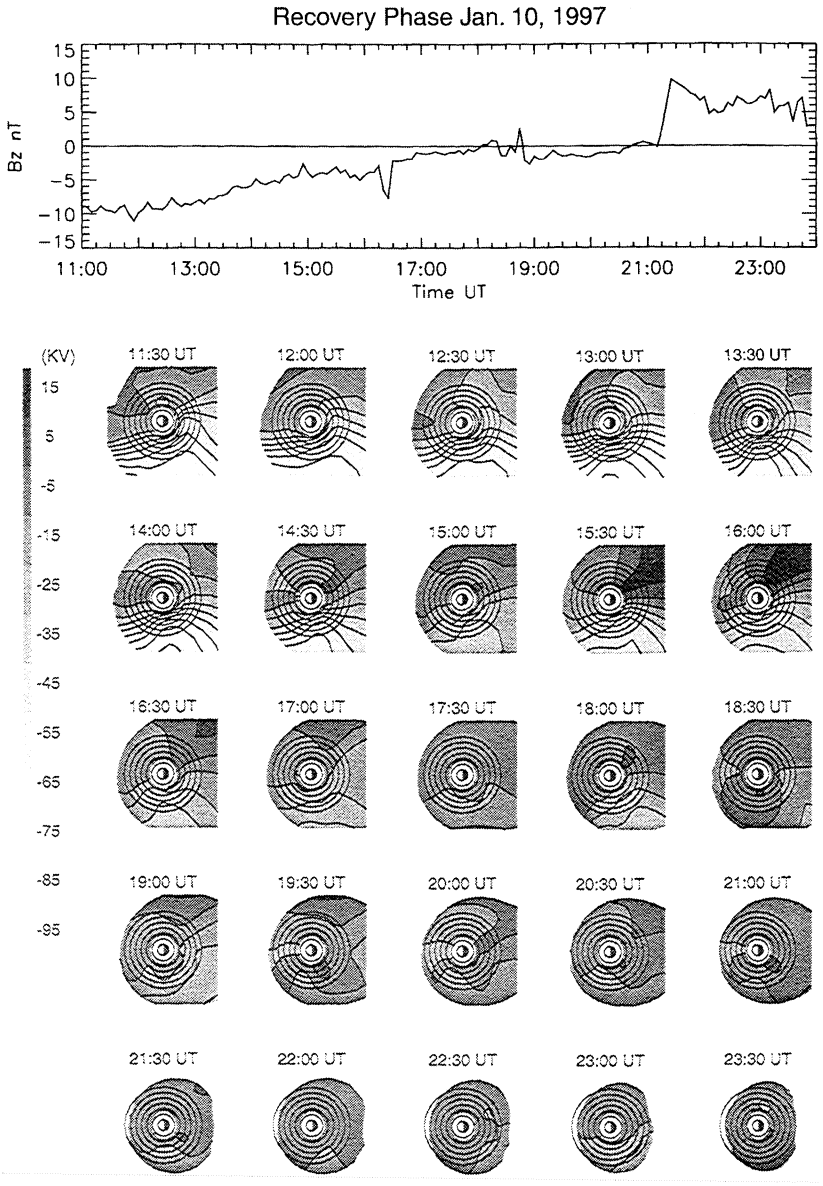

Figure 5. Dial plots of the MACEP equatorial potentials in the corotation frame for the storm recovery.

fidence level than the low-velocity data, but the low-velocity results have not been removed from the data sets. The universal time is noted in both plots; satellite 084 is ahead of 080 in orbit by about 2 hours. The velocities seen by both the 080 and 084 satellites show a pronounced increase in magnitude at around 0515 UT. This is directly associated with the pronounced and sustained southward shift in B_z. A second increase in convection velocities at the LANL spacecraft appears at ~0800 UT and ~0840 UT for satellites 080 and 084, respectively, and appears to be correlated with the region of minimum B_z and maximum convection electric field (Figure 4). Velocity measurements by satellite 084 in the storm main phase between 1630 LT and 1730 LT show a predominantly predawn to predusk flow which is consistent with the concept of a eastward rotation in the symmetry axis of the convection electric field to later local times (Figure 4). Unfortunately, measurements from satellite 080 at ~1000-1100 UT in this region (1630-1730 LT) are sparse and unreliable. Overall, both plots show a general sunward flow during the main phase of the storm on the dayside.

Figure 7 shows a qualitative comparison between the MACEP electric potential patterns and the LANL ion velocity vectors at selected times during the main phase of the January 10 storm. The convection electric field during the main phase is highly rotated on the dawnside pointing from noon to midnight. The electric field also penetrated to very low L values at all local times. Convective $\mathbf{ExB}/B^2$ velocities derived from the MACEP patterns are in approximate agreement with the direction of ion velocities obtained by the LANL spacecraft throughout the storm main phase.

A quantitative study of the comparison between the

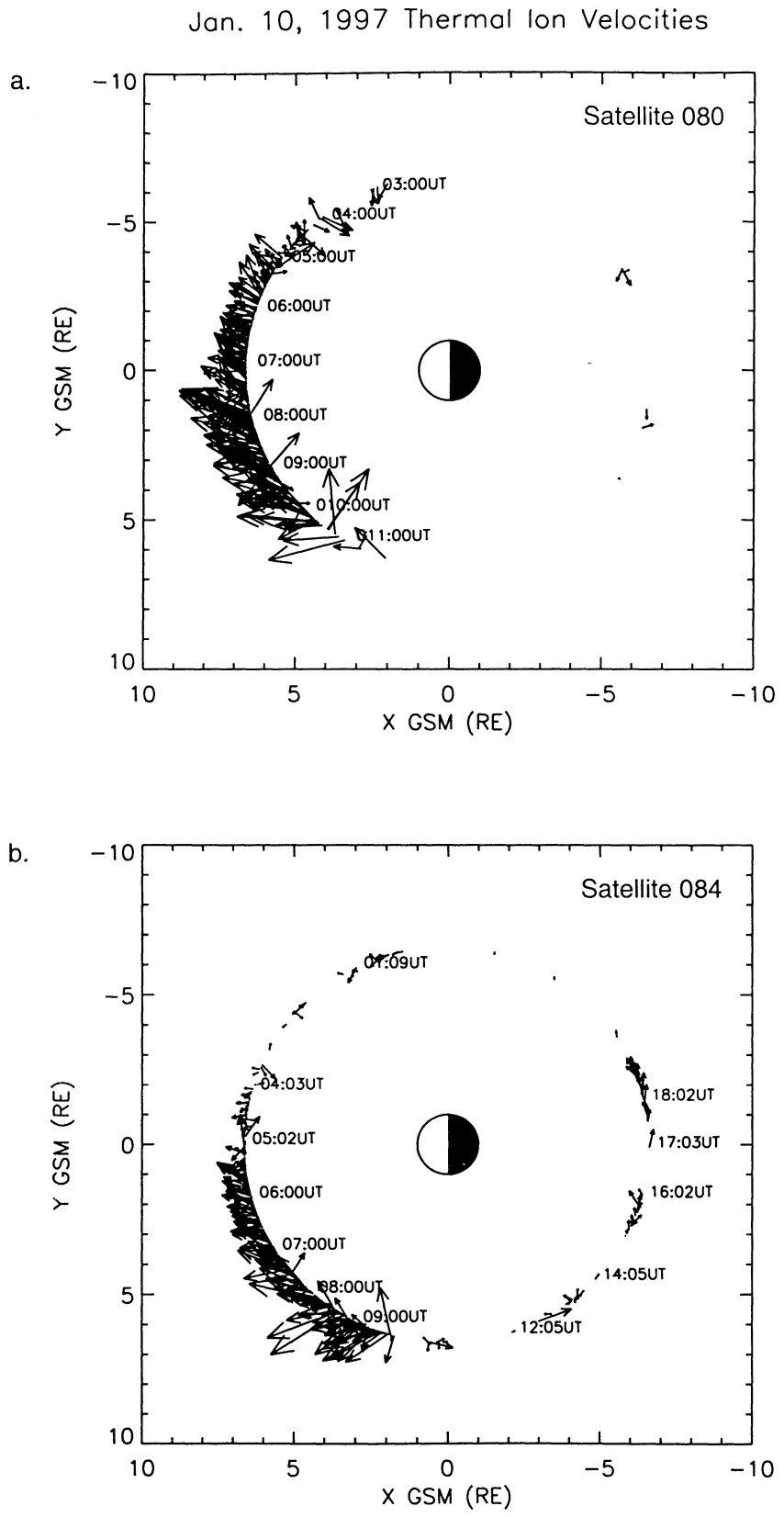

Figure 6. Thermal ion velocities in the corotation frame of reference obtained from two LANL satellites on January 10, 1997. Universal time is labeled in both plots. The increase in flow velocities at about 0520 UT and 0800 UT are associated with the variability in B_z.

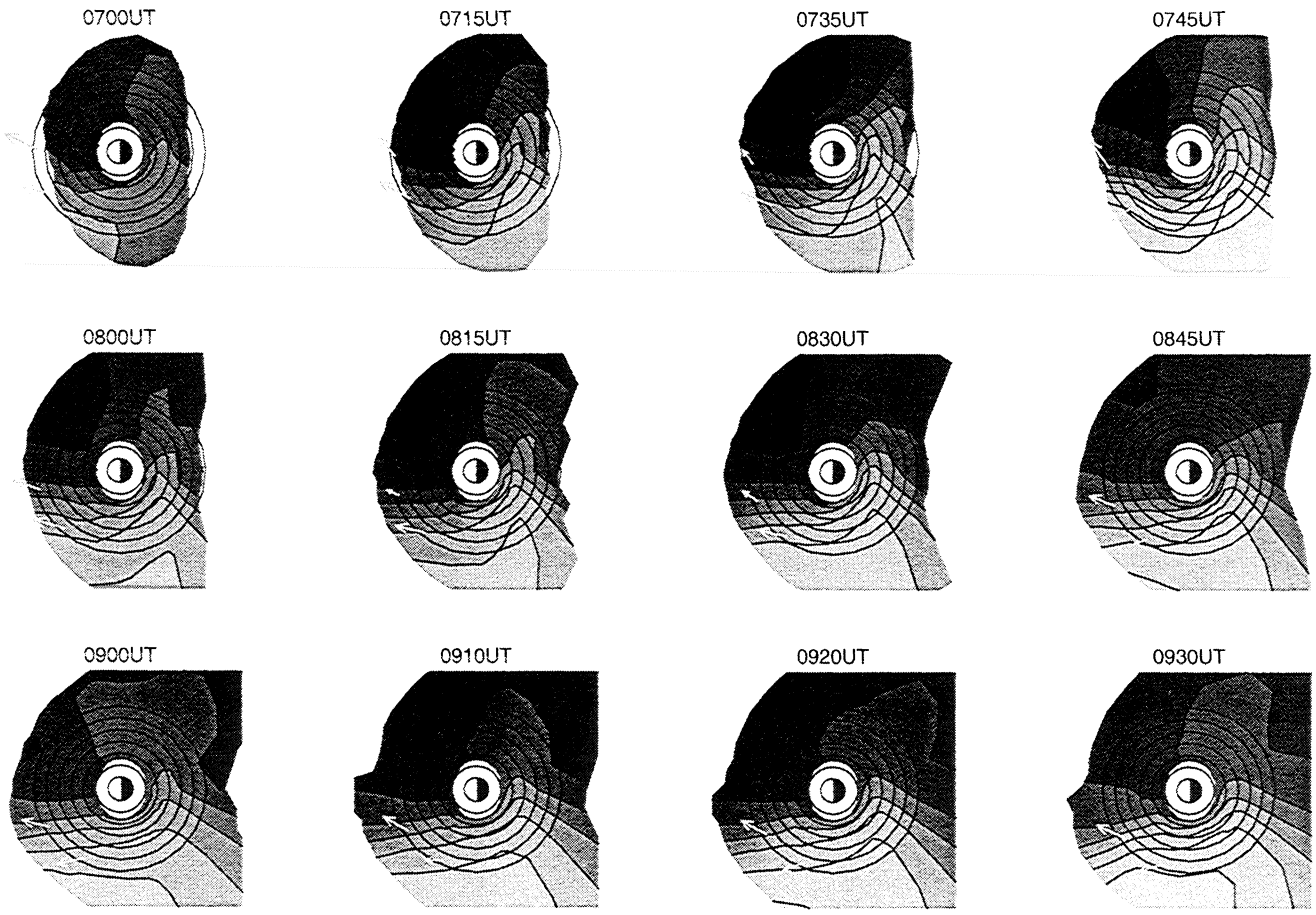

Figure 7. Qualitative comparison between selected MACEP patterns during the main phase of the storm and thermal velocities obtained from LANL spacecraft. The two arrows represent flows obtained from satellites 080 and 084.

magnitudes of the LANL velocities and MACEP velocities is shown in Figure 8. The two panels show a time series of the total velocity measured by the two LANL satellites at their corresponding positions shown in Figures 6a and 6b. MACEP represent a mapping of AMIE plus the penetration electric field (with a 90° westward rotation) associated with the asymmetric ring current while MACEP(−) shows a mapping of AMIE without the addition of the penetration electric field. Modeled velocities were calculated from $-\nabla\Phi \mathrm{x}\mathbf{B}/B^2$ at each point in time and space where LANL measurements were available at 5-min resolution. The results show that the MACEP(−) procedure follows the overall fluctuation trend and provides a realistic estimate of convection velocity during the storm recovery. However, MACEP(−) underestimates the magnitude of the convection velocity during the storm main phase. MACEP better estimates the magnitude of the convection velocity and gets closer to the baseline velocities measured by LANL. Neither MACEP nor MACEP(−) were able to reproduce the rapid fluctuations seen in the LANL velocities. These fluctuations are most likely due to inductive electric fields associated with magnetic field variations during geomagnetic activities. *Toivanen et al.* [1998] found that inductive electric fields are comparable in magnitude to the electrostatic fields during a substorm growth phase near the geosynchronous orbit. In a further study performed by *Lu et al.* [2000] the initial auroral brightening at the substorm onset appears to originate at $X = -5 \sim -7$ R_E. LANL measurements in Figure 8 show that the rapid fluctuations occur predominantly from 0700 UT to 1200 UT. An examination of CANOPUS magnetometer data reveals that a substorm occurred at around 0630 UT, and a large pressure pulse event occurred at around 1030 UT on January 10, 1997 [*Zesta et al.*, 2000]. Magnetic activities remain high from 0630 UT to 1200 UT. There was most likely strong inductive electric fields associated with this period which are not included in the MACEP or MACEP(−) electric fields. The exclusion

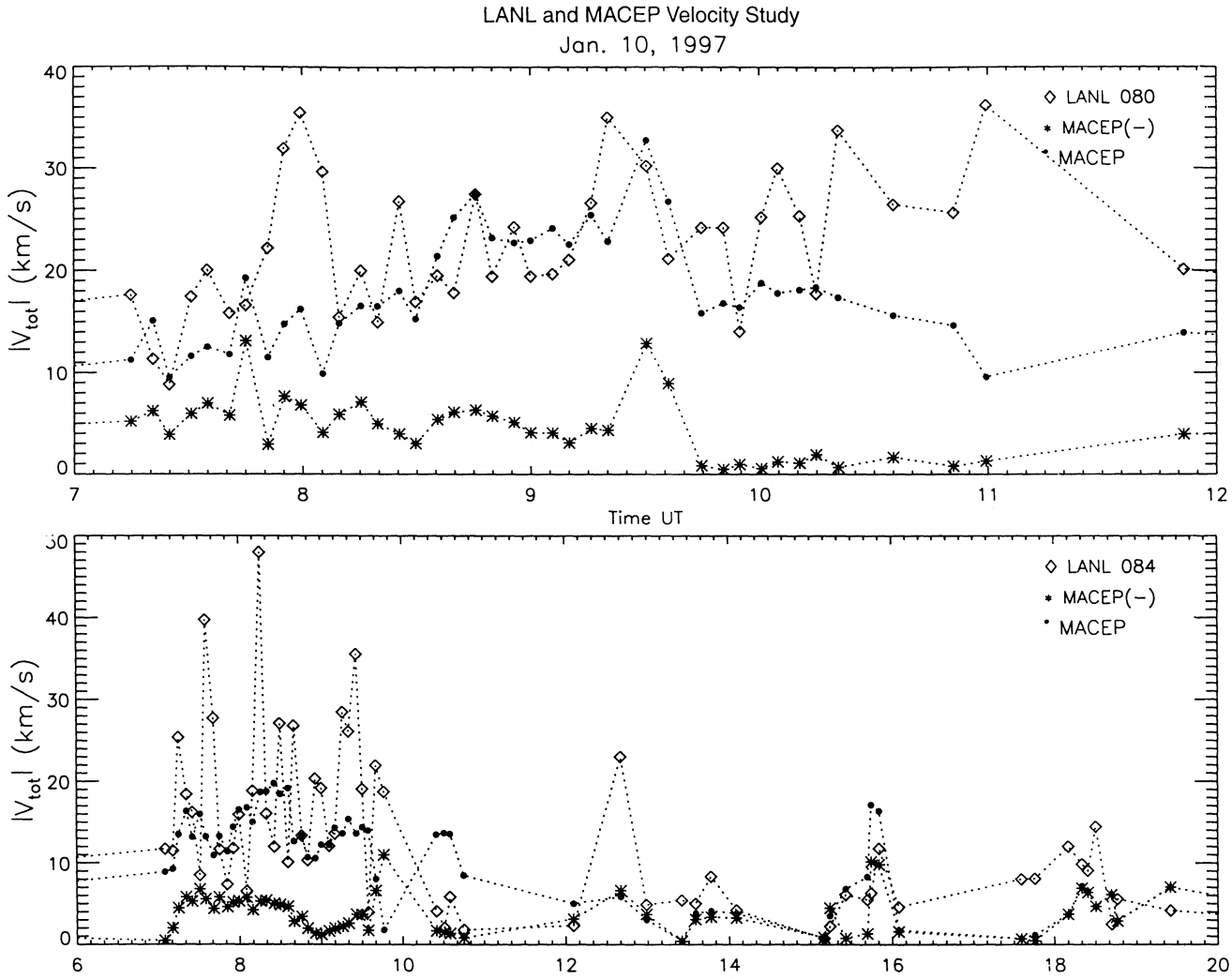

Figure 8. Total themal velocity time series at corresponding LANL 080 and 084 satellite positions compared with MACEP total velocity calculated with and without the addition of the penetration field due associated with the asymmetric ring current at 5-min data resolution.

of these inductive electric fields may very well be the cause of discrepancy seen in Figure 8. After the period of strong geomagnetic activities (>1200 UT), both MACEP and MACEP(−) velocities compared well with the measured LANL velocities.

5. Comparison of MACEP and Volland-Stern Electric Fields With POLAR/EFI Data

Electric field measurements from the electric field instrument on Polar have also been compared with MACEP and Volland-Stern electric fields on January 10, 1997. EFI measures three components of the electric field along the spacecraft trajectory. One component of the electric field lies along the spin axis; the other two components lie in the spin plane of the spacecraft. On January 10, the most reliable data were measured from the two probes in the spin plane. The electric field component along the direction of the spacecraft's velocity vector is calculated by using the two electric field components in the spin plane. Polar is in a near-dawn-dusk orbit on January 10, 1997. Two periods of the orbit when Polar traverses L shells that cross the equatorial plane between 2 and 10 R_E were used for this study. Instantaneous EFI electric field measurements (at 5-min intervals) were mapped to the equatorial plane by using the Tsyganenko 1996 magnetic field model employed by MACEP. The equatorial projection of the Polar orbit is plotted in the top panels of Figure 9. MACEP and Volland-Stern patterns are interpolated by using the Delaunay triangulation method to generate a finer grid system. The electric fields are then calculated along the equatorial positions of Polar for the corresponding times.

The bottom panels of Figure 9 show a comparison between the instantaneous EFI electric fields along the equatorial projection of Polar, the 5-min resolution MACEP, MACEP(−), and Volland-Stern electric fields at the corresponding positions. The 2-hour dawnside in-

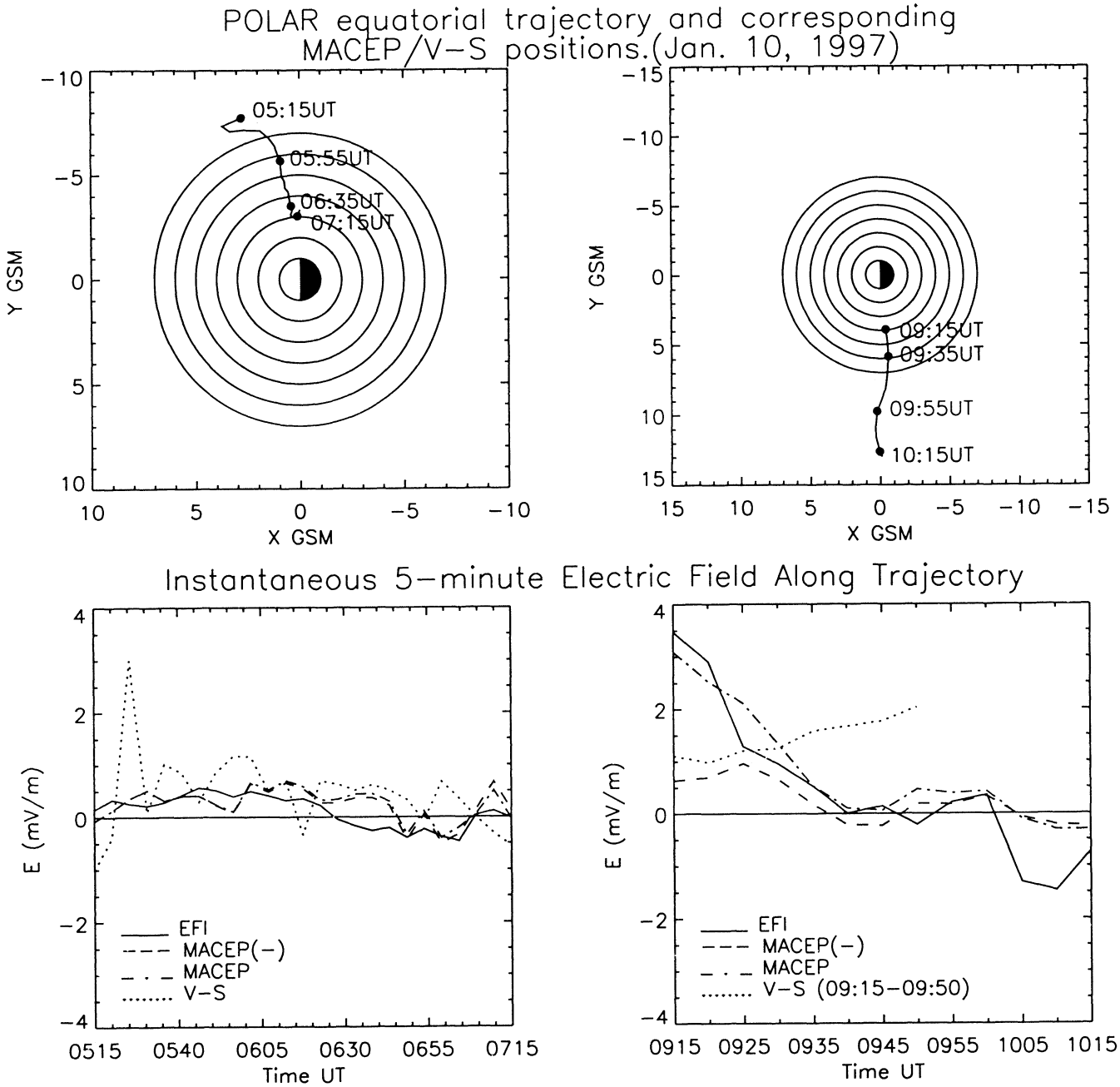

Figure 9. Polar trajectory mapped to the equatorial plane and the corresponding electric fields measured from EFI and calculated from MACEP and Volland-Stern patterns on January 10, 1997, during two time periods. All electric fields are in the corotation frame of reference.

bound pass corresponds to the prestorm and early storm main phase (0515-0715 UT). EFI measured relatively small fluctuating electric fields ($|E| < 0.6$ mV m^{-1}) which are in reasonable agreement with MACEP and MACEP(−) results shown in the bottom left panel. Both EFI and MACEP see a reversal of convection in the inner magnetosphere from 0640 UT to 0700 UT. MACEP and MACEP(−) show nearly identical results during this period because effects of the asymmetric ring current is minimal on the dawnside magnetosphere during moderate conditions. The Volland-Stern electric fields show much larger variations and tend to be larger in magnitude than either the EFI or the MACEP electric fields. Volland-Stern electric fields also do not show the field reversal at 0625 UT.

The bottom right panel of Figure 9 shows the duskside outbound pass during the main storm phase. Owing to data contamination at earlier times, only 1 hour of EFI data (0915-1015 UT) from this pass is used in this comparison. The Volland-Stern electric fields are only calculated from 0915 UT to 0950 UT owing to spatial limitations beyond 10 R_E. There is good agreement between EFI and MACEP electric fields. The reversal in convection after 1000 UT is seen in both EFI

and MACEP though MACEP underestimates the second field reversal by $\sim$1 mV m^{-1}. Extrapolation of the MACEP potential patterns into the region $L > 11$ may have contributed to the underestimation of the field reversal. While MACEP(−) significantly underestimates the electric field at low L from 0915 UT to 0925 UT, the MACEP results are in good agreement, which suggests that the electric fields associated with the asymmetric ring currents play an important role on the duskside magnetosphere during the storm main phase at low L.

Overall, there is generally good agreement between EFI and MACEP electric fields on the dawnside during the early main phase of the storm and at higher L (>4) on the duskside during the main phase of the storm. In contrast, the Volland-Stern model tends to overestimate electric field during prestorm conditions, and it gives no indication of the large penetrating fields during the storm main phase. Unfortunately, Polar data are extremely limited in both spatial and time coverage; a comparison study with MACEP patterns for other regions of the inner magnetosphere during other periods throughout this storm cannot be performed.

6. Comparison of MACEP, Weimer, and Volland-Stern Models

Figure 10 provides a comparison of the equatorial potenial patterns generated from the MACEP procedure, the *Weimer* [1996] ionospheric potentials, and the Volland-Stern model [*Volland*, 1973; *Stern*, 1975; *Maynard and Chen*, 1975] at various phases of the January 10, 1997, storm. This was a moderate storm with minimum *Dst* of -84 nT and a distinct storm sudden commencement, main phase, and recovery, making it a good case storm for modeling both quiet time (prestorm) and disturbed time (main phase) conditions.

In the *Kp*-dependent Volland-Stern model, the rotation of the axis of symmetry is a free parameter which is taken to be zero in this plot. All potentials are plotted on the same gray scale. Under quiet time conditions at 0000 UT, both the Weimer and MACEP potentials differ considerably from the *Kp*-dependent Volland-Stern pattern; the Volland-Stern potentials tend to overestimate the dawn-to-dusk potential drop consistent with the earlier study by *Baumjohann et al.* [1985]. At 0800 UT and 1200 UT, during the main storm phase, there is better agreement between the three potential patterns. However, there is a clear eastward rotation of the symmetry axis in MACEP mappings which is not as apparent in the mappings of Weimer potentials. Both the Weimer and MACEP potentials yield a larger dawn-to-dusk potential drop on the dayside than the Volland-Stern patterns. The three model/mappings show better agreement during the recovery phase of the storm (>1600 UT), but the westward rotation of the symmetry axis to earlier local times is only clearly seen in the MACEP pattern.

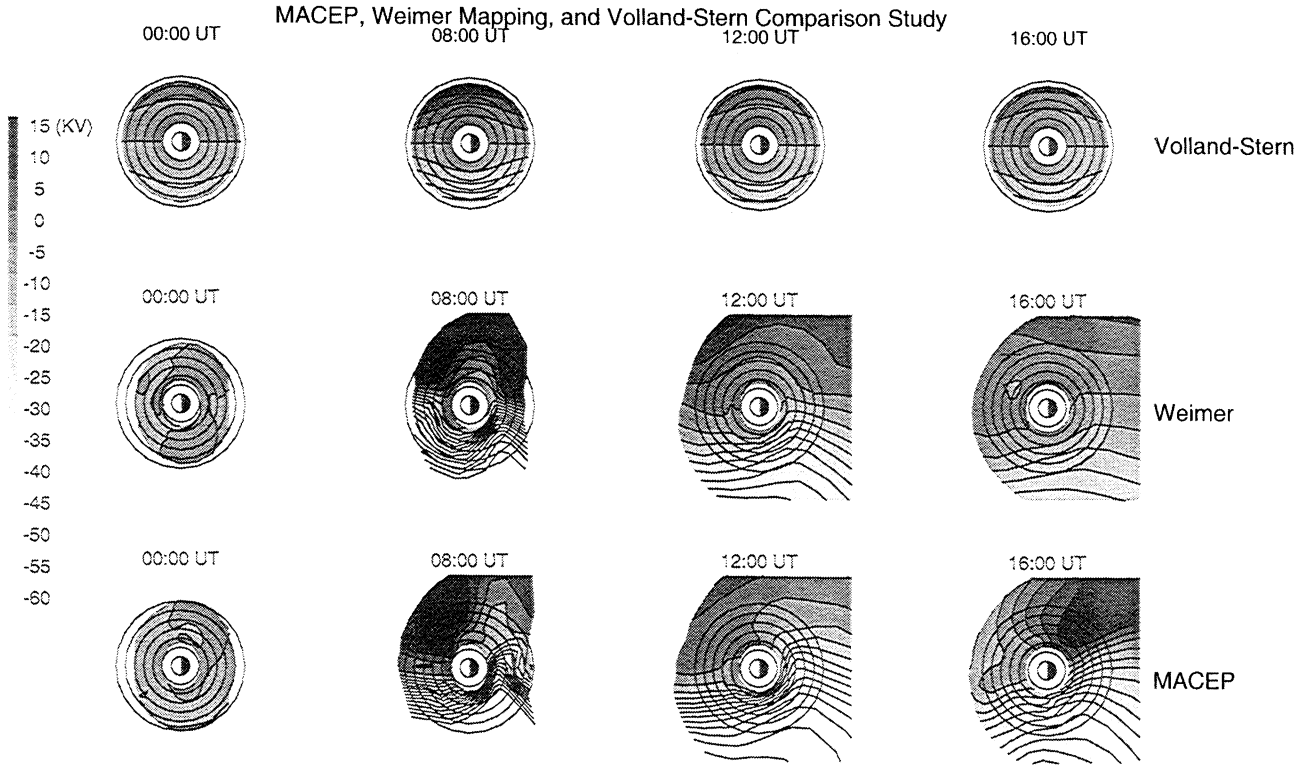

Figure 10. Comparison between the electric potentials generated from the (top) Volland-Stern model, (middle) Weimer mapping, and (bottom) MACEP for selected times throughout the storm.

7. Conclusions

Previous modeling studies of ring current development during magnetic storms have mainly been driven by a Volland-Stern type electric field. However, the present study clearly demonstrates that the convection electric field in the inner region of the magnetosphere cannot be represented simply by a Volland-Stern type model. The quiet time and disturbed time potential patterns as seen by both the Weimer mapping and MACEP are substantially different from those produced by the Volland-Stern model. Comparison with the EFI measurements also shows drastic differences to the Volland-Stern electric fields. The Weimer mapping shows only slight rotation of the axis of symmetry during both moderate and disturbed conditions. From the comparative study, it can be concluded that the Weimer mapping, due to its averaging nature, does not include the rapid time-varying features seen in MACEP. The MACEP procedure includes these rapidly varying features and has the potential to provide a more realistic method of studying inner magnetospheric convection and the evolution of the ring current population during geomagnetic storms.

Features in the MACEP electric field observed during the January 10, 1997, storm include penetration of convection to low L values during periods of southward B_z. As B_z continues to become more negative, E_{conv} intensifies at low L values. During moderately disturbed conditions, the axis of symmetry rotates westward to earlier local times, and overshielding is observed in association with northward turnings of B_z. As conditions become more disturbed, the axis of symmetry rotates eastward to much later local times. The controlling factor of the rotation may be linked to the asymmetric breakdown of the shielding electric field between the dayside and nightside magnetosphere. Periods of locally enhanced electric fields in the evening sector are seen in MACEP patterns which was also seen by other studies using in situ measurements. During the recovery phase of the storm, a region of potential enhancement is seen in the premidnight sector.

Although the MACEP procedure is limited by the imposed boundary conditions and data coverage available to AMIE, it has the potential to provide more accurate two-dimensional and time-dependent potential patterns than other methods currently being used to model storms. The adopted MACEP procedure maps AMIE potentials plus a penetration electric field associated with the asymmetric ring current (rotated by 90° such that the divergence of the current is on the duskside) down to the magnetosphere using the Tsyganenko 1996 magnetic field model. By applying MACEP to other storms we hope to obtain a better understanding of the features seen in inner magnetospheric convection. This should allow us to produce an improved empirical electric field model for the inner magnetosphere which can be used in future ring current modeling.

Acknowledgments. We are grateful to the following individuals and institutes for providing data for the AMIE potentials used in this study: G. Burns, D. Evans, J. Foster, R. Greenwald, M. Hairston, L. Hakkinen, K. Hayashi, T. Hughes, M. Lester, C. Maclennan, D. Milling, T. Moretto, L. Morris, S. I. Nechaev, V. Odintzov, V. Papitashvili, M. Pinnocky, J. Posch, A. S. Potapov, F. Rich, M. Ruohoniemi, G. Sofko, J. Thayer, O. Troshichev, G. van Beek, J. Villain, A. T. Weatherwax, K. Yumoto, and A. Zaitzev. The Polar UVI data were processed by D. Lummerzheim. The solar wind magnetic field and particle density data used in this study were provided by the MFI and SWE teams of the Wind satellite. The EFI data were provided by D. M. Ober and N. C. Maynard. We thank F. Mozer for the use of the EFI data. We thank A. J. Ridley and M. Liemohn for their collaboration efforts at improving AMIE and the use of their penetration electric field model. The authors would also like to thank R. A. Wolf, D. R. Weimer, L. R. Lyons, R. L. McPherron, N. C. Maynard, E. Zesta, C-P. Wang, and J. K. Arballo for helpful discussions. This study is supported in part by NASA grants NAG5-4680 and NAG5-7804 and NSF grant ATM97 29021. Work at HAO was supported in part by the NSF Space Weather program and by the NASA SEC Guest Investigator program.

Janet G. Luhmann thanks Douglas E. Rowland and another referee for their assistance in evaluating this paper.

References

Baumjohann, W., and G. Haerendel, Magnetospheric convection observed between 0600 and 2100 LT: Solar wind and IMF dependence, *J. Geophys. Res., 90,* 6370, 1985.

Baumjohann, W., G. Haerendel, and F. Melzner, Magnetospheric convection observed between 0600 and 2100 LT: Variations with *Kp*, *J. Geophys. Res., 90,* 393, 1985.

Chen, M. W., L. R. Lyons, and M. Schulz, Simulations of phase space distributions of storm time proton ring current, *J. Geophys. Res., 99,* 5741, 1994.

Farrugia, C. J., et al., Geoeffectiveness of three Wind magnetic clouds: A comparative study, *J. Geophys. Res., 103,* 17,261, 1998.

Fok, M.-C., T. H. Moore, J. U. Kozyra, G. C. Ho, and D. C. Hamilton, Three-dimensional ring current decay model, *J. Geophys. Res., 100,* 9619, 1995.

Foster, J. C., and F. J. Rich, Prompt midlatitude electric field effects during severe geomagnetic storms, *J. Geophys. Res., 103,* 26,367, 1998.

Foster, J. C., J. M. Holt, R. G. Musgrove, and D. S. Evans, Ionospheric convection associated with discrete levels of particle precipitation, *Geophys. Res. Lett., 13,* 656, 1986.

Jordanova, V. K., J. U. Kozyra, A. F. Nagy, and G. V. Khazanov, Kinetic model of the ring current-atmosphere interactions, *J. Geophys. Res., 102,* 14,279, 1997.

Jordanova, V. K., C. J. Farrugia, L. Janoo, J. M. Quinn, R. B. Torbert, K. W. Ogilvie, R. P. Lepping, J. T. Steinberg, D. J. McComas, and R. D. Belian, October 1995 magnetic cloud and accompanying storm activity: Ring current evolution, *J. Geophys. Res., 103,* 79, 1998.

Jordanova, V. K., R. B. Torbert, R. M. Thorne, H. L. Collin, J. L. Roeder, and J. C. Foster, Ring current activity during the early $B_z < 0$ phase of the January 1997 magnetic cloud, *J. Geophys. Res., 104,* 24895, 1999a.

Jordanova, V. K., L. M. Kistler, C. J. Farrugia, J. M. Quinn, M. F. Thomsen, G. D. Reeves, and J. D. Scudder, Temporal variability of the interplanetary parameters, the convection electric field and the ring current during March 10-15, 1998 (abstract), *Eos Trans. AGU, 80*(17), Spring Meet. Suppl., S298, 1999b.

Kistler, et al., Testing electric field models using ring current

ion energy spectra from the Equator-S Ion Composition (ESIC) instrument, *Ann. Geophys., 17,* 1611, 1999.

Kozyra, J. U., V. K. Jordanova, R. B. Horne, and R. M. Thorne, Modeling of the contribution of electromagnetic ion cyclotron (EMIC) waves to stormtime ring current erosion, in *Magnetic Storms, Geophys. Monogr. Ser.*, vol. 98, edited by B. T. Tsurutani, W. D. Gonzalez, and Y. Kamide, p. 187, AGU, Washington, D. C., 1997.

Kozyra, J. U., M.-C. Fok, E. R. Sanchez, D. S. Evans, D. C. Hamilton, and A. F. Nagy, The role of precipitation losses in producing the rapid early recovery phase of the great magnetic storm of February 1986, *J. Geophys. Res., 103,* 6801, 1998.

Lepping, R. P., et al., The WIND magnetic field investigation, *Space Sci. Rev., 71,* 207, 1995.

Liemohn, M. W., J. U. Kozyra, M. F. Thomsen, J. L. Roeder, G. Lu, J. E. Borovsky, and T. E. Cayton, The dominant role of the asymmetric ring current in producing the storm time *Dst*, J. Geophys. Res.,* in press, 2001.

Lu, G., M Brittnacher, G. Parks, and D. Lummerzheim, On the magnetospheric source regions of substorm-related field-aligned currents and auroral precipitation, *J. Geophys. Res., 105,* 18,483, 2000.

Lyons, R. L., and D. J. Williams, A source for the geomagnetic storm main phase ring current, *J. Geophys. Res., 85,* 523, 1980.

Maynard, N. C., and A. J. Chen, Isolated cold plasma regions: Observations and their relation to possible production mechanisms, *J. Geophys. Res., 80,* 1009, 1975.

Maynard, N. C., J. P. Heppner, and T. L. Aggson, Turbulent electric fields in the nightside magnetosphere, *J. Geophys. Res., 87,* 1445, 1982.

Maynard, N. C., T. L. Aggson, and J. P. Heppner, The plasmaspheric electric field as measured by ISEE 1, *J. Geophys. Res., 88,* 3991, 1983.

Ogilvie, K. W., et al., SWE, a comprehensive plasma instrument for the WIND spacecraft, *Space Sci. Rev.*, 71, 55, 1995.

Richmond, A. D., Assimilative mapping of ionospheric electrodynamics, *Adv. Space Res., 12* (6), 669, 1992.

Ridley, A. J., G. Crowley, and C. Freitas, An empirical model of the ionospheric electric potential, *Geophys. Res. Lett., 27,* 3675, 2000.

Rowland, D. E., and J. R. Wygant, Dependence of the large-scale, inner magnetospheric electric field on geomagnetic activity, *J. Geophys. Res., 103,* 14,959, 1998.

Stern, D. P., The motion of a proton in the equatorial magnetosphere, *J. Geophys. Res., 80,* 595, 1975.

Toivanen, P. K., H. E. Koskinen, and T. I. Pulkkinen, Mapping between the ionospheric and the tail electric fields in a time-dependent Earth's magnetosphere, *J. Geophys. Res., 103,* 9153, 1998.

Tsyganenko, N. A., Modeling the global magnetic field of the large-scale Birkeland current systems, *J. Geophys. Res., 101,* 27,187, 1996.

Volland, H., A semiempirical model of large-scale magnetospheric electric fields, *J. Geophys. Res., 78,* 171, 1973.

Weimer, D. R., Models of high-latitude electric potentials derived with a least error fit of spherical harmonic coefficients, *J. Geophys. Res., 100,* 19,595, 1995.

Weimer, D. R., A flexible, IMF dependent model of high-latitude electric potentials having "space weather" applications, *Geophys. Res. Lett., 23,* 2549, 1996.

Wolf, R. A., The quasi-static (slow flow) region of the magnetosphere, in *Solar Terrestrial Physics*, edited by R. L. Carovillano and J. M. Forbes, pp. 303-368, D. Reidel, Norwell, Mass., 1983.

Wygant, J., D. Rowland, H. J. Singer, M. Temerin, F. Mozer, and M. K. Hudson, Experimental evidence on the role of the large spatial scale electric field in creating the ring current, *J. Geophys. Res., 103,* 29,527, 1998.

Zesta, E., H. J. Singer, D. Lummerzheim, C. T. Russell, L. R. Lyons, and M. J. Brittnacher, The effect of the January 10, 1997, pressure pulse on the magnetosphere-ionosphere current system, in *Magnetospheric Current Systems, Geophys. Monogr. Ser.*, vol. 118, edited by S. Ohtani, R. Fujii, M. Hesse, and R. L. Lysak, p. 217, AGU, Washingtone, D. C., 2000.

Zhou, X.-W., C. T. Russell, G. Le, and N. A. Tsyganenko, Comparison of observed and model magnetic fields at high altitudes above the polar cap: POLAR initial results, *Geophys. Res. Lett., 24,* 1451, 1997.

A. Boonsiriseth and R. M. Thorne, UCLA Department of Atmospheric Sciences, Math Sciences 7127, MS 7984, 405 Hilgard Avenue, Los Angeles, CA 90095. (e-mail: amyb@atmos.ucla.edu; rmt@atmos.ucla.edu)

V. K. Jordanova, University of New Hampshire, Space Science Center, Durham, NH, 03824. (e-mail: vania@unhedi1.sr.unh.edu)

G. Lu, High Altitude Observatory, P.O. Box 3000, Boulder, CO 80307-3000. (e-mail: ganglu@hao.ucar.edu)

D. M. Ober, Mission Research Corp., Suite 302, Nashua, NH 03062. (e-mail: Dober@mrcnh.com)

A. J. Ridley, University of Michigan, Space Research, Ann Arbor, MI 48109. (e-mail: ridley@umich.edu)

M. F. Thomsen, Los Alamos National Laboratory, Space and Atmospheric Sciences MS D466, Los Alamos, NM, 87545. (e-mail: mthomsen@lanl.gov)

(Received September 10, 1999; revised January 4, 2001; accepted February 20, 2001.)